Kinetic Hole Burning, Hole Filling, and Conformational Relaxation in Heme Proteins: Direct Evidence for the Functional Significance of a Hierarchy of Dynamical Processes[†]

Jerry Huang, Andrew Ridsdale, Jiaqien Wang, and Joel M. Friedman*

Department of Physiology and Biophysics and the W. M. Keck Biomolecular Laser Research Center, Albert Einstein College of Medicine, Bronx, New York 10461

Received January 3, 1997; Revised Manuscript Received September 22, 1997[⊗]

ABSTRACT: Band III is a disorder and conformation-sensitive near-infrared (∼760 nm) charge transfer absorption band characteristic of equilibrium and nonequilibrium five coordinate ferrous high-spin hemes. The time evolution of this absorption band subsequent to photodissociation of six coordinate ferrous hemoglobin or myoglobin can provide detailed information regarding conformational relaxation, including the thermally driven fluctuations that result in the transition from inhomogeneous to homogeneous ligand rebinding kinetic. Such time-resolved measurements over a range of temperatures are difficult due to long sample recovery times at cryogenic temperatures. A new rastoring technique that allows for the rapid movement of a large optically accessible cryostat is used in combination with nanosecond time-resolved near-infrared absorption spectroscopy to generate band III as a function of time for the photoproducts of the carbon monoxide derivative of adult human hemoglobin (COHbA) and, to a more limited extent, horse myoglobin (COMb). The measurements are made over a wide range of temperatures extending from well below the solvent (75% glycerol:water) glass transition at ∼180 K to ambient temperatures. Three temperature- and/or viscosity-dependent phenomena are observed. At the highest temperatures, only conformational relaxation is observed for the 75% glycerol sample. At very high viscosity (≥400 cp), conformational relaxation slows dramatically, and both kinetic hole burning followed by the filling in of the "hole" (dynamic hole filling) are observed. As the temperature is lowered, conformational relaxation slows and finally ceases. Kinetic hole burning and dynamic hole filling as well as additional broadening of band III are observed down to 140 K. The observation of kinetic hole burning (KHB) is indicative of the sample being inhomogeneous on the time scale of the ligand rebinding giving rise to KHB. The onset of hole filling is a direct manifestation of the thermal homogenization of the initial inhomogeneous distribution of conformational substates responsible for KHB. The observed dynamics are used to explain the inverse temperature effect associated with the non-Arrhenius slow down of geminate rebinding above ∼180 K. The inverse temperature effect appears to arise not only from the onset of conformational relaxation but also from the increase in the rate on thermal averaging of the initial inhomogeneous distribution of conformational substates.

A detailed molecular level description of how proteins function is a major objective of molecular biophysics. An important and often essential first step in pursuing this daunting task is the determination of the equilibrium structures through techniques such as X-ray crystallography and NMR. It is becoming ever more apparent that the static equilibrium structures are often just the starting point, in that protein motions and nonequilibrium populations are key concepts that need to be included and explored in order to understand protein function.

Relatively recently, proteins have started to be perceived as dynamically active macromolecules with multiple layers of complexity. Several concepts have emerged and have been examined, spurred on largely by the pioneering and persistent work of Frauenfelder and co-workers (Austin et al., 1975; Frauenfelder & Wolynes, 1985; Frauenfelder et al., 1988, 1991; Frauenfelder, 1995).

Two of the most basic concepts are (1) proteins are inherently disordered or "glass-like" in that they have many locally frustrated (non-energy-minimized) structures that are constrained against relaxation and (2) these structural constraints are hierarchical with respect to both protein structure and dynamics (Ansari et al., 1985, Frauenfelder et al., 1985, 1991; Frauenfelder, 1995). For example, a multimeric protein may have multiple quaternary states. Each quaternary state can accommodate a range of tertiary structures. In turn, each tertiary state, defined by some average position of helices and other macroelements that define protein structure, can then provide the boundaries for a distribution of subconformations or conformational substates (cs) associated with more local aspects of structure. These cs then provide the boundary conditions for a next lower level of complexity which has its distribution of cs. Associated with each layer or tier of conformational organization is a comparable tier of dynamics. The possible interconversions among the conformational substates of each tier define the corresponding tier of dynamics. Although there is clear evidence that protein structure and dynamics are organized hierarchically based on cryogenic studies

[†] This work was supported through NIH (GM 44343) and the W. M. Keck Foundation.

* Author to whom correspondence should be addressed.

[⊗] Abstract published in *Advance ACS Abstracts,* November 15, 1997.

S0006-2960(97)00027-5 CCC: $14.00

(Ansari et al., 1985, 1987; Iben et al., 1989; Leeson & Wiersma, 1995), the link to functionality at ambient temperatures remains elusive.

Several operational elements are required in order to adequately address the study of protein motion in a way that exposes the hierarchy of conformations and dynamics as well as its relationship to functionality. One needs a spectroscopically accessible system that can be driven from equilibrium fast enough to allow for the probing of relaxation dynamics over several decades in time. A functional process is needed that occurs over a comparable time scale in order to follow the effect of the dynamics on reactivity (e.g., ligand binding). The temporal profile of the functional process should contain "relaxation footprints" that reflect the influence of a relaxation event as it is occurring. Ideally, both the dynamics and the functional process should be tunable and dissectable through both manipulation of solvent conditions and systematic perturbation of conformation through mutagenesis, species differences, or binding of substrates.

Geminate recombination (GR) in heme proteins is a near perfect model reaction for such studies (Austin et al., 1975; Alpert et al., 1979; Duddell et al., 1979; Friedman & Lyons, 1980; Henry et al., 1983; Hofrichter et al., 1983; Jongward et al., 1988; Murray et al., 1988). In heme proteins, GR refers explicitly to the recombination process that occurs from within the protein prior to any ligand escape into the surrounding solvent. Ligand dissociation can be triggered nearly instantaneously (Martin et al., 1983) using a short laser pulse to photodissociate a heme-bound ligand. Depending upon the ligand, the protein and the solvent conditions, the geminate phase can occur on time scales as short as a few picoseconds and extend out to seconds or longer (at cryogenic temperatures).

The kinetics and yield of GR in heme proteins are sensitive to the local conformation of the heme and its proximal (Friedman et al., 1985; Friedman, 1994) and distal environment (Olson & Phillips, 1996). Furthermore, the pattern of kinetics is highly reflective of conformational disorder. Below the glass transition of the solvent, the time dependence of the GR is consistent with there being a frozen distribution of conformational substates each having its own characteristic exponential rebinding kinetics that obeys the anticipated Arrhenius dependence on temperature (Austin et al., 1973). Well above the glass transition, the rebinding kinetics are reflective of a conformationally averaged population having an average energy barrier dictating the kinetics.

A breakdown of the Arrhenius activation behavior is observed for GR as the increasing temperature approaches the glass transition (Austin et al., 1973). Instead of the anticipated continued acceleration with increasing temperature, there is a marked slow down in the GR process. In carbonmonoxy myoglobin (COMb), this non-Arrhenius behavior, called the inverse temperature effect, has been attributed to the onset of a relaxation that results in an increase in the kinetic barrier controlling ligand rebinding (Agmon & Hopfield, 1983; Steinbach et al., 1991).

A direct link between conformation, conformational disorder, conformational relaxation, and GR is provided through the properties of a near-IR porphyrin to iron charge transfer absorption band called band III (Iizuka et al., 1974, Eaton et al., 1978). Band III appears at approximately 760 nm for five coordinate high-spin ferrous heme. In the absence of significant changes in the polarity of the distal heme pocket (Kiger et al., 1995), the peak wavelength of band III is reflective of proximal heme pocket environment (Chavez et al., 1990) and correlates with the kinetic barrier controlling ligand rebinding (Cambell et al., 1987; Agmon, 1988; Chavez et al., 1990; Steinbach et al., 1991; Srajer & Champion, 1991). Changes in the peak position of Mb*, the photoproduct of COMb, as the temperature is raised to and above the solvent glass transition have been linked to the origin of the inverse temperature effect (Steinbach et al., 1991; Srajer & Champion, 1991). Measurements at cryogenic temperatures on the change in the line shape of band III for both Mb* (Cambell et al., 1987; Agmon, 1988; Chavez et al., 1990; Steinbach et al., 1991; Srajer & Champion, 1991) and Hb* (Chavez et al., 1990; Srajer & Champion, 1991) reveal a kinetic hole burning effect that indicates that both the disordered conformational coordinate and the resulting distribution of kinetic barriers responsible for the distributed GR kinetics at temperatures below 100 K map onto the inhomogeneous line shape of band III. As a result of this mapping, there is an asymmetric loss of line shape as the low barrier population of cs rebind before the higher barrier populations.

In this present study, geminate rebinding measurements and time-resolved studies on band III are used together to expose functionally relevant tiers of relaxation phenomena in both the photoproducts of COHbA (carbonmonoxy adult human hemoglobin) and COMb. The peak wavelength and line shape of band III are followed as a function of time (10−1000 ns) over a temperature regime extending from 293 to 140 K or lower in some instances. A new methodology for rastoring the cryostat is used to insure that each pulse/probe pair of 8 ns pulses encounters a recovered liganded sample.

COHbA is focused upon instead of the more traditionally studied COMb system because the yield of geminate rebinding for HbA is considerably larger than for native forms of mammalian Mbs (Friedman & Lyons, 1980; Hofrichter et al., 1983; Henry et al., 1983; Murray et al., 1988), and the dynamic behavior appears richer (Friedman, 1994). Both factors facilitate achieving the goal of exposing the interplay between dynamics and geminate rebinding on the faster time scales. Limited data sets on both COMb (horse heart) in 75 and 95% glycerol:water and COHbA in 95% glycerol:water are used for comparative and evaluative purposes. The photoproducts at time t of COHbA and COMb are to be referred to as Hb*(t) and Mb*(t), respectively.

The results obtained demonstrate temperature- and viscosity-dependent phenomena occurring over several temporal domains. Kinetic hole burning, fluctuation-induced conformational averaging, and conformational relaxation are all observed in real time. The time ordering and the solvent dependencies of these processes indicate that the dynamics of the proximal heme pocket are organized hierarchically. In addition, the inverse temperature effect in photodissociated COHbA is seen to originate at least in part from temperature and/or viscosity dependence of the thermally induced conformational averaging time, i.e., the time over which the protein solution starts to appear homogeneous with respect to the iron-associated kinetic barrier controlling GR.

METHODS AND MATERIALS

Sample Preparation. Hemoglobin, isolated from human blood and purified using standard procedures, was provided as a kind gift from Prof. S. Acharya (Division of Hematology, Albert Einstein Collage of Medicine). For this study, the HbA was stored in liquid nitrogen as the O_2 form in 0.05 M Bis-Tris buffer at pH 6.5 until ready to use. Myoglobin derived from horse skeletal muscle (Sigma) was dissolved in 0.05 M phosphate buffer at pH 7.0 and then passed through a 0.2 μm filter (Schleicher & Schuell) before further use. The CO derivatives were prepared by first flushing the solution with helium gas and then adding a slight excess of sodium dithionite solution freshly prepared under anaerobic conditions. The sample is then saturated with CO for about an hour in an ice bath. The HbA sample was prepared at a concentration 0.86 mM in heme and Mb at 0.68 mM in 75% (v/v) glycerol and sealed in a 0.25 cm path cell. The absorption spectra of samples were measured before and after each data acquisition on a Perkin Elmer UV−vis spectrometer to determine the oxidation state and ligation status of the sample.

Nanosecond Time-Resolved Band III Studies. A Janis closed cycle He cryostat with large optical windows, mounted on a computer-controlled rastoring stage (UNIDEX 12, Aerotech), was used in the temperature-dependent studies. The sample is cooled slowly and stabilized at the desired temperature for at least 1.5 h before measurements. Temperature is controlled by a Lakeshore temperature controller (Model 330) within 0.01 K. Rastoring of the sample is used to insure that each photolysis pulse encountered a fresh ligand-bound sample in order to minimize light-induced relaxation, sample degradation, and photoproduct buildup.

The experimental setup used in the nanosecond time-dependent study includes two Nd:YAG lasers (SURELITE, Continuum) that have an output at 532 nm and a pulse width of 6−8 ns. The two lasers are externally triggered with variable relative delays by a pulse generator (Model DG535, Stanford Research System). The time delay between the two laser pulses is monitored by a photodiode connected to an oscilloscope (Model 2235A, Tektronix). The photolysis pulse (5.0 mJ/pulse at 532 nm) is first passed through a 450−700 nm depolarizer and then focused onto the sample. The 532 nm output of the other laser is focused onto a 2 mm diameter glass capillary tube containing a 15 °C circulating mixture of dyes [see Sassaroli and Rousseau (1987)]. The fluorescence output from the dye mixture becomes the source of a probe beam that provides a high spectral density in the 700−800 nm region. The output from the capillary tube at 700−800 nm is passed through a red filter and a 650−1100 nm depolarizer before being focused onto the sample. A dichroic mirror (532 nm/700−800 nm) is used to facilitate overlap of the two pulses.

A 0.27 meter monochrometer (600 grooves/mm) with the entrance slit set at 0.1 mm (Model 270 M, Spex) and a mounted unintensified diode array with 1024 pixels (RY-1024G/B, Princeton Instrument) is used for dispersion of the transmitted light and acquisition of data. The typical integration time on the diode array is 10 min or less. The data acquisition at different time delays is temporally randomized and taken several times. The reference spectrum (unphotolyzed sample) is obtained by blocking the photolysis pulse of by using a negative time delay (probe pulse before photolysis pulse). The logarithm of the reference divided by the spectrum at time t is used to generate the absorption spectrum of the photoproduct at time t. The composite effective resolution for the above setup is approximately 0.5 nm.

The absorption spectra are processed by first performing a baseline subtraction. Gaussian fits are used on the flat baseline spectra to help determine the peak position, intensity, and the full-width at half-maximum.

Geminate Recombination (10 ns Resolution) as a Function of Temperature. The flash photolysis apparatus used for rebinding rate studies employs the doubled output of a Nd:YAG laser (SURELITE, Continuum) at 532 nm to photolyze the sample and the attenuated cw output of a HeCd laser at 441.6 nm to monitor the recombination via changes in sample absorbance. The photolysis pulse of ~8 ns in duration is focused to a diameter of approximately 2 mm at the sample. To achieve 100% photolysis within the illuminated sample volume, the pulse energy is increased until the amplitude of the change in the transmittance signal saturates. Saturation typically requires approximately 2 mJ/pulse. The unfocused probe beam is first passed through the sample collinearly with the photolysis beam, then spectrally separated from the 532 nm light using colored glass filters and a short monochromator, and finally detected with a photomultiplier tube (Hamamatsu R928). For each laser shot, the detector output is digitized with a 500 MHz oscilloscope (Lecroy), resulting in a trace with 50 000 points at 10 ns separation. Traces for 100 laser shots are averaged. The data are converted from transmittance to absorbance by taking a logarithm, subtracting a baseline, and normalizing.

Picosecond Pump-Probe Measurement of Rebinding Kinetics Monitoring the Soret Band at Room Temperature. A Coherent Mira Ti:Sapphire oscillator operating at a center wavelength of 838 nm is used to seed a Ti:Sapphire regenerative amplifier after pulse stretching through a grating system. The regenerative amplifier is pumped by a Q-switched, frequency doubled YLF laser (Optronix) and produces pulses of up to 30 μJ at 1500 kHz. The seeding and extraction of pulses from the amplifier is driven by a Pockels cells, which is controlled by custom built electronics.

The amplified pulses are recompressed using a grating system (to approximately 200 fs full-width half-max.). They pulses are frequency doubled through a BBO crystal (to 419 nm center wavelength). The doubled and nondoubled pulses are separated by a dichroic beam splitter and the blue light directed through delay line and then through a chopper which blocks every other pulse. These pulses constitute the pump beam. The remaining 838 nm light, doubled via a second BBO crystal constitutes the probe beam. Both beams pass a short-wave-pass filter before interaction with the sample to preclude the possibility of exposure to any remaining 838 nm light.

After interaction with the sample (2 O.D. at 419 nm in a 2.5 mm thick rotating cell), the probe beam is detected with a Hamamatsu model photomultiplier whose output is directed to a Stanford Research Systems SR530 model lock-in amplifier which is synchronized with the chopper driver (i.e., only signal modulated at 750 kHz is detected).

The sample cell is in contact with a heat sink which is maintained near 295 K with water circulating from a temperature-controlled bath.

RESULTS

Temperature Dependence of Hb(10 ns) and Mb*(10 ns): Band III Intensities.* Figure 1 shows a plot of the relative absorption intensity as a function of temperature of band III for Hb*(10 ns) and Mb*(10 ns) and the 10 ns photoproduct of COHbA and COMb, respectively, in a 75% glycerol:water solution. It can be seen that the absorption intensity drops for Hb*(10 ns) in going from 295 to 180 K and then begins to increase with further reduction in temperature. In contrast, under identical conditions the intensity consistently increases with decreasing temperature for Mb*(10 ns).

Temperature Dependence of the Geminate Recombination for COHbA. Figure 2a shows that, upon lowering the temperature from 300 to 220 K, the nanosecond through microsecond geminate phase of CO recombination shows an increase in both apparent rate and yield for the geminate rebinding occurring within the first 100 ns. Figure 2b demonstrates the Arrhenius-type slowing of rebinding upon lowering the temperature beyond 180 K. The rebinding curves shown in Figure 2 have been normalized with respect to the initial amplitude at ~10 ns. The unnormalized initial amplitudes at time $t = 0 \pm 10$ ns decrease in going from 300 to 220 K and then show a slow increase upon lowering the temperature further. These results suggest that upon reduction in temperature a subnanosecond geminate phase decreases the observed 10 ns yield. Since the dominant temperature effect upon lowering the temperature from 295 to ~200 K is a dramatic several orders of magnitude increase in viscosity (Ansari et al., 1992), the geminate rebinding in COHbA at ambient temperature was examined on the subnanosecond time scale as a function of viscosity (from less than 100 to ~1000 cP) in order to determine if increased viscosity could account for an increase in the geminate yield at 10 ns.

Viscosity Dependence of the Picosecond Geminate Recombination in COHbA. Results from ultrafast recombination experiments are shown in Figure 3. The geminate recombination of CO to hemoglobin at room temperatures is either slightly enhanced or unchanged by the addition of glycerol to the 75% level. The further addition of glycerol to concentrations of 90, 95, and 98% (by volume) increases the rate of recombination and the total fraction of CO which undergoes geminate recombination within 2 ns. The results indicate that the increase in the geminate rate and yield occurs at the 90% glycerol level with little change upon further addition of glycerol.

Temperature Dependence of Hb(10 ns) and Mb*(10 ns): Band III Line Shapes.* Figure 4a shows band III for Hb*(10 ns) as a function of temperature for the 75% glycerol sample. The intensities have been normalized to allow for a direct comparison of peak positions and line shapes. In going from 295 to 180 K, the most pronounced change is the loss of the red edge of band III. Further reduction in temperature below 180−140 K results in no additional change. Rastoring of the sample below 140 K proved difficult because of the appearance of cracks and fissures in the sample. Accurate measurements of time-dependent

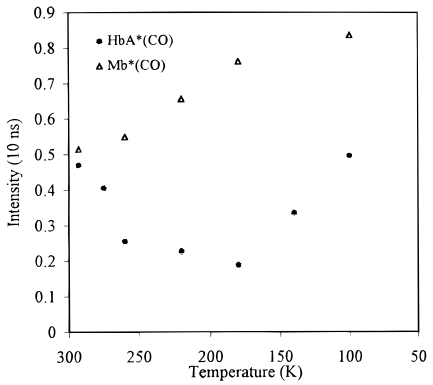

FIGURE 1: A comparison of the temperature dependence of the peak intensity of band III as a function of temperature for the photoproduct at 10 ns of the carbonmonoxide derivative of HbA, human adult hemoglobin, and Mb, horse heart myoglobin. In both cases, the solvent is a 75% glycerol:water mixture. The spectral intensity of both samples has been arbitrarily set to the same value of 0.5 at 293 K.

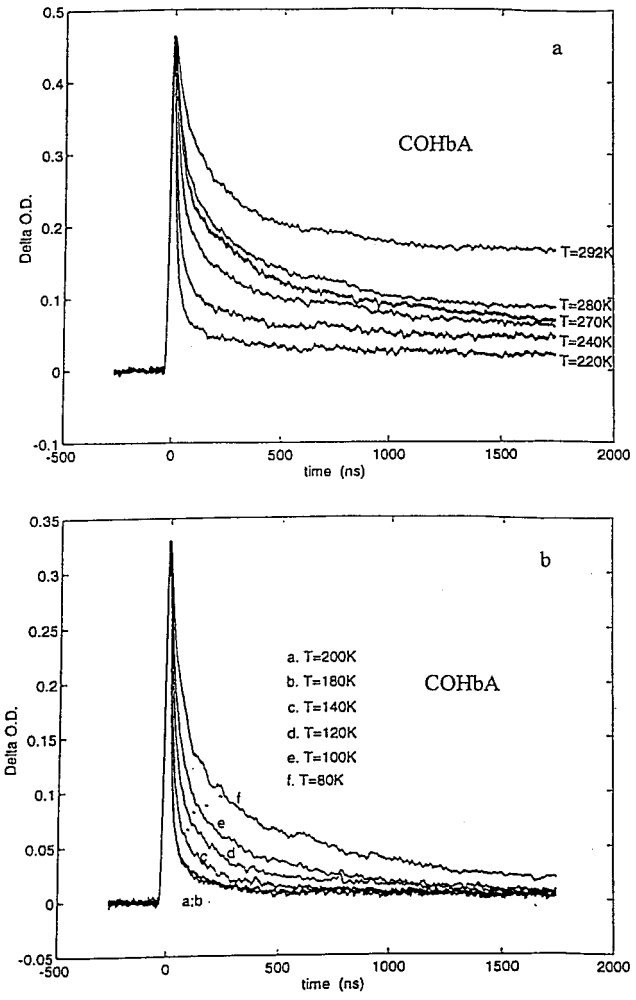

FIGURE 2: The temperature dependence of the geminate recombination in COHbA in 75% glycerol:water. Figure 2a covers the temperature regime from ambient to 220 K. Due to space constraints, the rebinding curve for 260 K is not labeled. It is situated directly below the 270 K rebinding curve. Figure 2b covers the temperature regime from 200 to 80 K. In both figures, the initial change in optical density has been normalized (see text for a discussion of this point).

phenomena below 100 K also proved difficult for Hb* because of a light-induced relaxation which resulted in the appearance of a significantly blue-shifted band III after

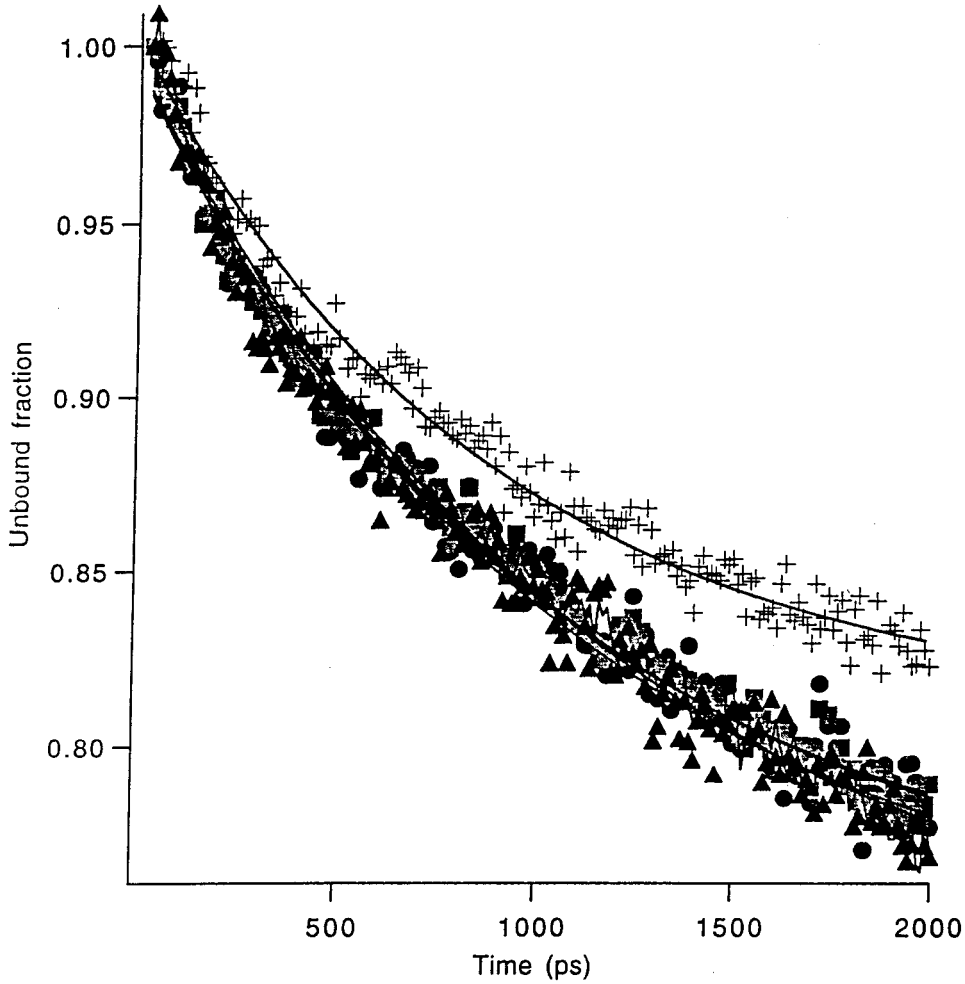

FIGURE 3: Fast phase of CO geminate recombination with HbA in high concentrations of glycerol. Aqueous recombination cannot be distinguished from that in 75% glycerol (crosses). Recombination at higher concentrations of glycerol are shown by the filled symbols (90%, circle; 93%, squares; and 97%, triangles). Fitted single exponential curves are also shown. Glycerol concentrations are ±0.5% and are by volume.

prolonged illumination at temperatures near 100 K (manuscript in preparation).

Figure 4b shows that the Mb*(10 ns) spectrum does not show the highly asymmetric loss of the red edge as seen for Hb*(10 ns). There is narrowing that includes both the red and blue side of the line. In addition, the peak wavelength shifts toward redder wavelengths with decreasing temperatures. It appears that the red shift from ~762 to 765 nm occurs over a relatively narrow temperature window near 200 K. The deoxy forms of both proteins show a progressive blue shift with decreasing temperature that persists below 180 K. In addition, the width of band III for the deoxy derivatives continues to narrow with decreasing temperature over the entire temperature range. It should be noted that without rastoring the sample, the line narrowing and peak shifts seen for Hb*(10 ns) and Mb* were either eliminated or reduced at temperatures around 180 K.

Hb in 75% Glycerol at 293 K (Figure 5).* As the intensity decreases over the first few hundred nanoseconds, there is only a very small change in peak position with no change in line shape. There is a progressive blue shift of the entire band from 765 nm at 10 ns to ~762 nm at 10 μs after photodissociation (not shown). Full relaxation to the equilibrium deoxy value of 759 nm takes well over 100 μs as seen in Figure 5.

Hb in 95% Glycerol at 293 K (Figure 6).* There is an initial progressive loss of the red edge in the normalized spectra which is readily apparent at 40 ns. The progressive loss of the red edge is followed by a progressive filling in of the lost edge followed by continued broadening. By 100 ns, the lost red edge has been filled in and by 5 μs, the band is broader than it was at the initial 10 ns point. There is no blue shifting at long times (5 μs). The spectrum of the equilibrium deoxy species in 95% glycerol is also shown. It should be noted that the corresponding deoxy spectrum in 75% glycerol is at ~759 nm in contrast to the 761 nm for the 95% sample, an effect possibly due to enhanced osmotic stress influencing the globin in an as yet unspecified fashion.

Mb in 75% Glycerol at 293 K.* The normalized band III for the deoxy Mb, Mb*(10 ns), and Mb*(80 ns) show very little difference in peak frequency (~762 nm); however, the photoproduct spectra are very slightly red shifted relative to the deoxy species (spectra not shown).

Mb in 95% Glycerol at 293 K.* Whereas band III in 75% glycerol is very nearly relaxed at 10 ns, in 95% glycerol, the red-shifted band III at 10 ns exhibits a pronounced 1−2 nm relaxation over a 100 ns interval to approach a near equilibrium value. Within our signal to noise ratio, it is not possible to determine the extent to which there is a remaining relaxation beyond the first 100 ns.

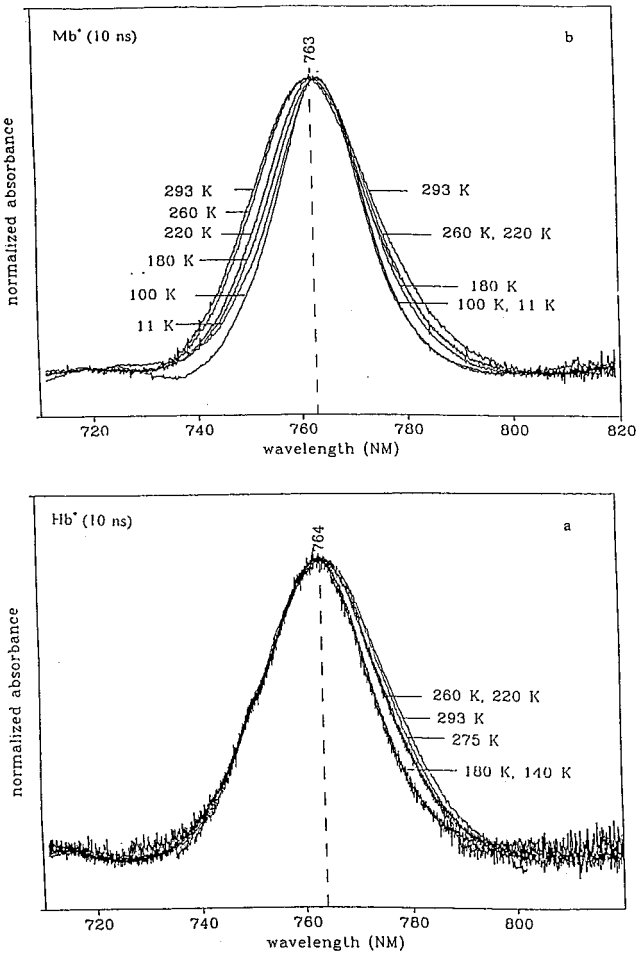

FIGURE 4: The temperature dependence of the line shape and peak position of intensity normalized band III for: (a) Hb*(10 ns), the photoproduct at 10 ns for COHbA and (b) Mb*(10 ns), the photoproduct at 10 ns of horse heart COMb. In both cases, the solvent is 75% glycerol.

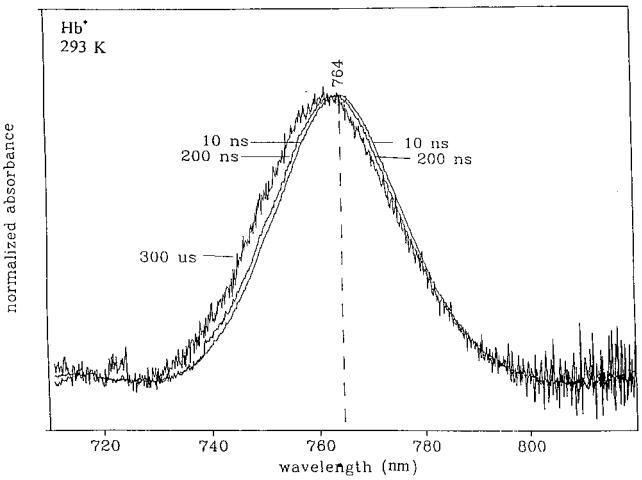

FIGURE 5: The time dependence of the intensity normalized band III for Hb* at 293 K in 75% glycerol.

Hb in 75% Glycerol at 275 K.* A substantial decrease in the intensity of band III as a function of time is observed (not shown). The time evolution of the band III peak position slows compared to 293 K in that no change is observed over the first 200 ns. The peak wavelength remains at ~764 nm. A small blue shift of the entire band does become apparent at later times. Similar results but with indications of line shape changes at early times are seen for

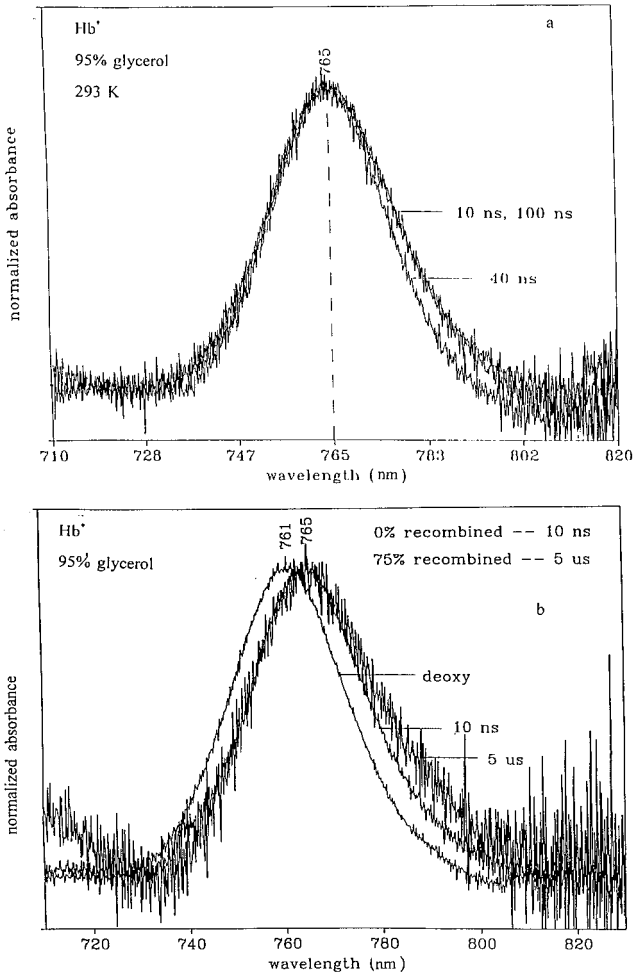

FIGURE 6: The time dependence of intensity normalized band III for Hb* in 95% glycerol at 293 K. Figure 6a shows the early time changes in line shape, whereas in Figure 6b, the comparison is shown of the 10 ns spectrum with both the equilibrium deoxy species and the photoproduct at 5 μs.

Hb* at 260 K. These line shape changes which become more distinct at lower temperatures are discussed in the subsequent paragraph.

Hb in 75% Glycerol at 180 K (Figure 7).* There is a rapid drop in the band III intensity over the first few tens of nanoseconds subsequent to photodissociation. The initial 10 ns spectrum at 180 K is considerably narrower and more blue shifted than the 220 K 10 ns spectrum. Continued blue shifting of the entire band is apparent at 30 ns (Figure 7a). At 50 ns, band III has broadened relative to the 30 ns spectrum. The red edge returns to the same position as for the initial 10 ns spectrum but the blue edge is much broader. In Figure 7b, it can be seen that at 300 ns the broadening has increased on both the red and blue edges. It appears that compared to the initial 10 ns spectrum the broadening is skewed toward the blue but by 500 ns (not shown) the resulting broadened peak appears more symmetric, although the extreme low intensity of the band precludes an accurate line shape analysis. Thus, between 10 and 500 ns, the peak position appears to initially blue shift but then recovers. The time evolution of band III at 220 K (not shown) shows similar narrowing followed by broadening.

Hb in 75% Glycerol at 140 K (Figure 8).* Compared to the 180 and 220 K series, the drop in intensity for band III at 140 K is slower. The 10 ns spectrum is narrowed and

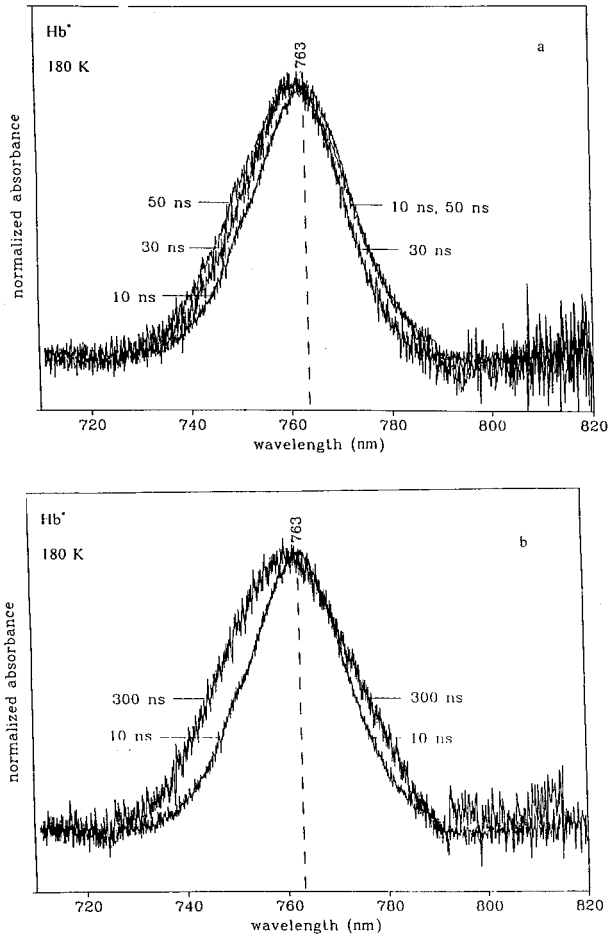

FIGURE 7: (a, b) Time evolution of intensity normalized band III for Hb* in 75% glycerol at 180 K.

blue shifted as at 180 K. The spectrum continues to blue shift with time out to ~80 ns (Figure 8a). The spectrum then begins to shows signs of red edge broadening at 100 ns (Figure 8b). The broadening continues (Figure 8c), and by 3 μs, the red edge has broadened significantly compared to the initial 10 ns spectrum.

Mb in 75% Glycerol at Cryogenic Temperatures.* As the temperature is lowered from 295 to 180 K, there is a progressive separation of the peak wavelength between band III for the equilibrium deoxy species and Mb*(10 ns). At intermediate temperatures such as 260 K, relaxation of band III can be observed at 80 ns. Figure 9 shows the normalized band III spectrum for equilibrium deoxyMb, Mb*(10 ns), and the Mb*(80 ns) at 180 and 100 K, respectively. At 180 K, it is readily apparent that the photoproduct is red shifted by several nanometers relative to the deoxy species. It can be seen that the 80 ns photoproduct spectrum has lost part of its red edge compared to the 10 ns spectrum and is therefore narrower. The 100 K spectrum of the photoproduct at 10 ns is peaked at the same wavelength as at 180 K but is narrower. The band broadens both on the red and blue sides in going to 80 ns. The 80 ns spectrum at 100 K is comparable in width to the 10 ns spectrum at 180 K. It is noted that the 100 K sample is not being rastored, and as a consequence, there may be some artifact due to that small fraction of the sample that has not recovered between pairs of pulses. The contribution to the spectra at 100 K of photodissociated sample that does not recover between pairs of pulses would be expected to broaden the line shape of

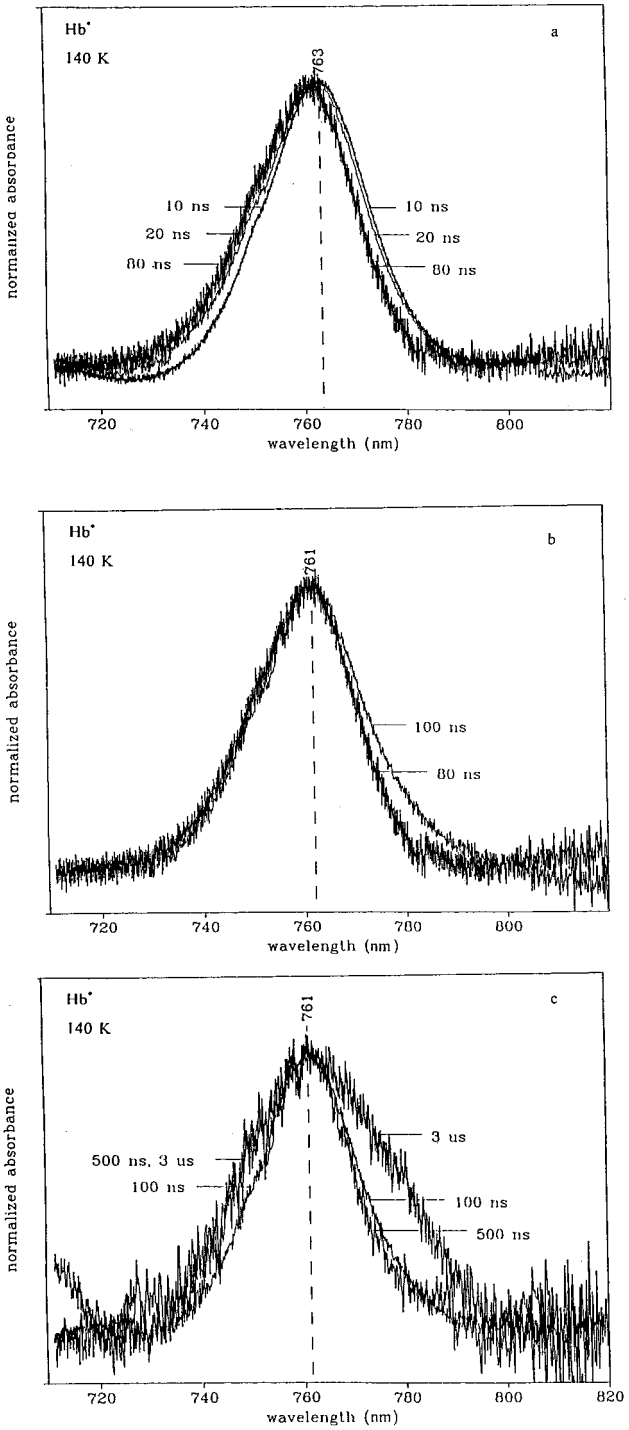

FIGURE 8: (a−c) Time evolution of intensity band III for Hb* in 75% glycerol at 140 K.

band III at both 10 and 80 ns. Thus, the observed narrowing of band III at 100 K for Mb*(10 ns) is a lower limit for the extent of line broadening.

DISCUSSION

The time and temperature dependent changes in band III for Hb* reveal the following phenomena: (1) an intensity decrease for band III [Hb*(10 ns)] in going from 300 to 180 K, followed by an intensity increase with further reduction in temperature; (2) a relatively slow viscosity dependent symmetric relaxation of band III toward the equilibrium peak position; (3) an asymmetric shift of band III to the blue due to a loss of the red edge of the band III line shape, which is

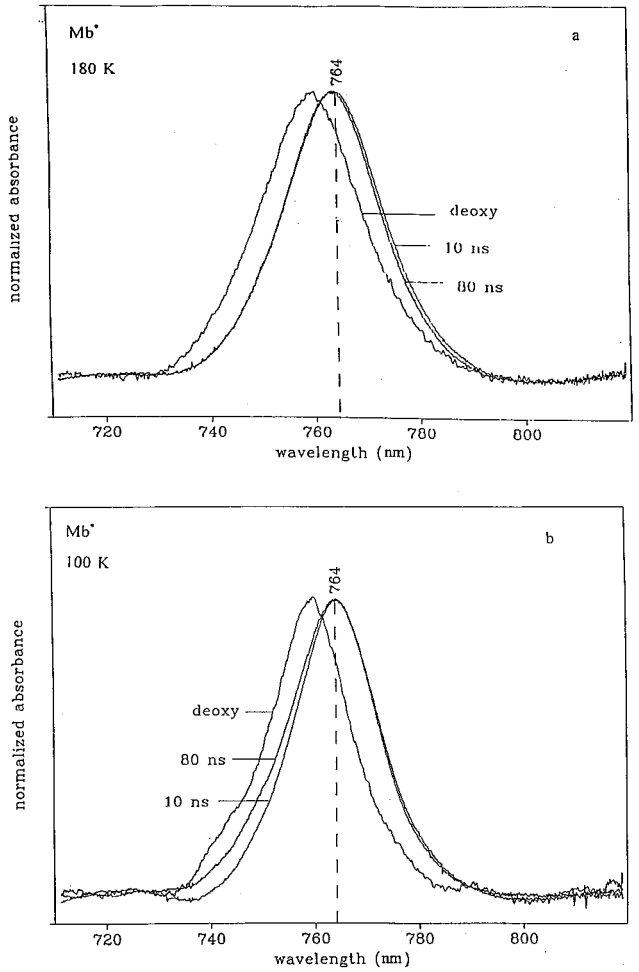

FIGURE 9: Time evolution of band III for Mb* in 75% glycerol at (a) 180 K and (b) 100 K. The spectrum of the equilibrium deoxy derivative is also shown for comparative purposes.

observable either at reduced temperatures or at substantially elevated viscosities; and (4) line broadening subsequent to the above described asymmetric blue shift, that fills in the lost red edge of band III resulting in a reversal of the blue shift.

The following discussion is an attempt to assign physical processes to the above spectroscopic observations.

Origin of the Temperature-Dependent Intensity Change in Band III for Hb.* In general, most five coordinate ferrous heme proteins that have been examined display a band III that undergoes an intensity increase upon reduction in temperature. This phenomenon has been observed in deoxy HbA (Cordone et al., 1986), deoxy Mb (Cupane et al., 1988; Gilch et al., 1996), and the deoxy and photoproduct forms of the dimeric clam hemoglobin from *Scapharca i.* (Huang et al., 1996). It thus appears that the decrease in integrated intensity (the first moment, M_0) for Hb*(10 ns) in going from 300 to 180 K is atypical.

The fraction of the photoproduct population undergoing geminate rebinding within 100 ns greatly increases in dropping the temperature to 180 K. The decrease with temperature in the amplitude of the initial optical density change upon photodissociation parallels the decrease in the intensity of band III for Hb*(10 ns). These results suggest that the decrease in the intensity of band III is due to an increase in the overall average rate of the geminate process with decreasing temperature which is sufficient to produce a substantial amount of recombination on the sub-10-ns time scale. In aqueous buffer at ~300 K there is only ~5% geminate rebinding occurring for COHbA during the first few nanoseconds (Green et al., 1978; Friedman et al., 1985; Scott et al., 1985). The femtosecond excitation results presented in the present work clearly demonstrates that increasing the viscosity of the solvent can enhance the geminate yield over the first several nanoseconds.

The femtosecond time-resolved results show that, at 295 K, the glycerol-enhanced subnanosecond geminate phase occurs when the concentration of glycerol exceeds approximately 90%. The viscosity of glycerol:water mixtures increases dramatically at 293 K as the percent glycerol (by weight) increases from 75% (<<100 cp) to 95% (~600 cP) to 98% (~1100 cP). It is thus likely that the glycerol effect on the GR begins to be appreciable when the viscosity reaches several hundred centipoise. Such viscosity values are readily achieved for the 75% glycerol sample as the temperature drops below 280 K.

The above results together support the idea that the effect of decreasing the temperature is related to the concomitant increase in viscosity as previously proposed based on COMb studies (Ansari et al., 1992, 1994). The anomalous decrease in the intensity of band III for Hb*(10 ns) in going from 300 to 180 K can now be ascribed to a viscosity-induced increase in the geminate rebinding occurring within the pulse duration of the excitation. Mb*(10 ns) in 75% glycerol does not show this effect because the intrinsic rate of CO rebinding is slower than for COHbA. The increase in the integrated intensity of band III for Hb*(10 ns) with decreasing temperatures after reaching a minimum (at around 180 K for 75% glycerol) is ascribable to a combination of a slow down of the fast geminate phase and of an intensity increase that is typically observed for other five coordinate heme systems.

The Origin of Temperature-Dependent Line Shape Changes in Mb(10 ns): A Viscosity-Induced Slow Down of Relaxation.* Band III for Mb*(10 ns) shows narrowing upon temperature reduction, but with what appears to be a drastic reduction in the blue edge. This asymmetric narrowing creates a red-shifted band when compared to the higher temperature species (~765 nm versus 762 nm). Although the blue edge exhibits the greater reduction, the narrowing also includes the red edge as well. Thus upon lowering the temperature to 200 K, band III of Mb*(10 ns) becomes red shifted with respect to the equilibrium *(deoxy)* species at the same temperature. This red shift is maintained for cryogenically trapped Mb* (Iizuka et al., 1974) at temperatures below 60 K where, under weak illumination conditions, relaxation of band III is not observed (Campbell et al., 1987).

At 300 K, the initial picosecond MbCO photoproduct has a red-shifted band III, similar to what is observed at cryogenic temperatures, which relaxes to near completion within tens of picoseconds (Lim et al., 1993; Jackson et al., 1993). The current and previous (Franzen & Boxer, 1997) results on Mb* in a viscous solvent at temperatures above the glass transition indicate that, at higher viscosity, the picosecond relaxation of the red-shifted form of Mb* can be significantly slowed so as to be observable on the nanosecond time scale. Increasing the viscosity even further by embedding MbCO in a room temperature glass (trehalose) having viscosities exceeding 10^{13} cP results in the absence of detectable band III relaxation out to 10^3 ns (Levin &

Friedman, unpublished results). Thus, the temperature effect on the band III wavelength of Mb*(10 ns) is due to the temperature-dependent increase in the viscosity that slows and eventually stops the relaxation process responsible for the decrease in the band III peak wavelength difference between Mb* and the equilibrium deoxy species.

The Origin of Temperature-Dependent Line Shape Changes in Hb(10 ns): Kinetic Hole Burning Induced Line Shape Changes.* The behavior of band III for Hb*(10 ns) is very different from that of Mb*(10 ns). Upon reduction in temperature, band III for Hb*(10 ns) appears to lose only the red edge. This red edge loss follows the decrease in intensity of band III, which has been attributed to a temperature/viscosity enhanced geminate phase occurring faster than the observation time scale of 10 ns (vide supra).

This behavior for band III of Hb*(10 ns) is very similar to what is observed in steady state measurements at temperatures below 100 K for Mb* (Campbell et al., 1987; Agmon, 1988; Steinbach et al., 1991; Ahmed et al., 1991; Srajer, & Champion, 1991) and Hb* (Chavez et al., 1990; Ahmed et al., 1991). In those studies, a progressive loss of the red edge of band III is observed with increasing amounts of rebinding. This phenomenon is termed kinetic hole burning (KHB).

KHB occurs when a spectral band characteristic of either the ligand-bound or ligand-free species is inhomogeneously broadened due to conformational degrees of freedom linked to ligand reactivity. Through this linkage, each inhomogeneous spectral element contributing to the overall line shape appears or disappears at a rate characteristic of the conformational substate population giving rise to that element. As a consequence, the line shape will change asymmetrically during a rebinding process if the cs have different rebinding rates. The magnitude of the effect is limited by homogeneous broadening from such phenomena as lifetime broadening and pure dephasing. The appearance of KHB is a direct indication that, on the time scale of the rebinding process, the sample remains conformationally inhomogeneous with respect to the degrees of freedom responsible for the variation in rebinding rates. Conversely, the loss of KHB reflects conformational averaging occurring faster than the rebinding process.

Band III for five coordinate high-spin ferrous heme is centered at ~760 nm. The ligand-bound species display no well-defined spectral features in that region. The initial steady state studies show that band III for Mb* and Hb* is inhomogeneously broadened at temperatures well below 100 K and that the red edge populations are associated with conformational substates that have the lowest kinetic barriers for rebinding (Campbell et al., 1987; Agmon, 1988, 1990; Chavez et al., 1990; Steinbach et al., 1991, Nienhaus et al., 1992; Srajer & Champion, 1991). Several of these studies reveal a direct mapping of the distribution of enthalpic barrier heights for rebinding onto the inhomogeneous line shape of band III (Agmon, 1988, 1990; Steinbach et al.; 1991; Nienhaus et al., 1992; Srajer & Champion, 1991). The extent of KHB is limited by a rather large homogeneous width for band III.

It was demonstrated that the line shape changes taking place below 80 K in the weak excitation limit originate almost entirely from KHB and not relaxation (Campbell et al., 1987; Chavez et al.,1990). Subsequent studies have shown the existence of light-induced relaxation caused by repetitive excitation of the sample (Nienhaus et al., 1994; Abadan et al., 1995; Ahmed at al.,1991). Under these conditions, a blue shift in band III occurs due to relaxation induced not as a direct bulk thermal effect but as a byproduct of the photon excitation process (Nienhaus et al., 1994), which produces local transient heating at the heme.

The observed temperature-dependent line shape changes in Hb*(10 ns) in the present study are consistent with KHB. Not only is there more of a red edge loss as the fast rebinding increases, but the blue shift and the line narrowing appear correlated, another indicator of KHB (Agmon, 1988, 1990). The absence of KHB for Mb*(10 ns) is readily explained by Mb* having a distribution of enthalpic barriers that are skewed toward higher energies compared to Hb*. Thus, there is minimal rebinding during the 7 ns excitation in the COMb case and, consequently, no observation of KHB on this time scale. The loss of the red edge seen in the 80 ns band III spectrum at 180 K for Mb* (see Figure 9a) is, however, likely due to KHB occurring on a slower time scale.

Time-Dependent Changes in Band III as a Function of Temperature: Tertiary Relaxation in Hb.* At 293 K, band III for Hb* in 75% glycerol shifts from ~764 to ~761 nm within 10 μs. This behavior is similar to the aqueous phase relaxation of band III reported earlier (Sassaroli & Rousseau, 1987). The blue shifting of band III is consistent with tertiary relaxation of the photodissociated ligand-bound R state to the deoxy R state (Scott & Friedman, 1984; Jayaraman et al., 1995). There is no indication of KHB since there is no line narrowing and the shifting does not appear to correlate with geminate rebinding occurring over the tens to hundreds of nanoseconds time scale.

Increasing viscosity slows down the nanosecond tertiary relaxation as seen for band III in the 95% glycerol sample where the same peak position is observed for Hb*(5 μs) and Hb*(10 ns) and for the time evolution of the iron-proximal histidine stretching mode in the resonance Raman spectra (Findson et al., 1988).

Time-Dependent Changes in Band III as a Function of Temperature: KHB and Dynamic Hole Filling. Although the peak position of band III of Hb* in 95% glycerol is the same at early and late delays, it is clear that there are line shape changes at intermediate times that cause transient peak shifts. Initially, band III for the 95% glycerol sample shows a loss of the red edge on the tens of nanoseconds time scale. This loss of the red edge is readily assignable to KHB. The KHB is followed by a filling in of the "hole" at 80 ns and continues out to the microsecond regime. The final line shape at 5 μs is broader than the initial one associated with Hb*(10 ns). The observed filling in of the kinetically hole-burned red edge and the further broadening is attributable to thermal fluctuations inducing transitions among the different cs that contribute to the inhomogeneous broadening of band III. The broadening of band III and the loss of the KHB-induced "hole" represent the temporal transition over which the sample becomes homogenous with respect to the degree of freedom responsible for the band III line shape. This hole filling process will be referred to a dynamic hole filling (DHF) since it is dynamical motion of the protein (thermal fluctuations) and not the ligand binding kinetics (as in KHB) that is assumed to be responsible for this effect.

It thus appears that increasing the viscosity effectively stops the large amplitude tertiary relaxation [as reflected in the peak wavelength of band III and ν(Fe-His)] and slows

conformational averaging to the point where nanosecond KHB and the subsequent DHF can be observed. It is important to note that DHF represents a real time window into the process that determines on what time scale the sample appears inhomogeneous, i.e., conformationally averaged with respect to the degree of freedom responsible for KHB in band III. The temperature and viscosity dependence of the conformational averaging times observed from DHF appear similar to those derived from double pulse excitation protocols used in conjunction with geminate rebinding studies on COMb (Tian et al., 1992, 1996).

Intensity normalized band III for Hb* at 220, 180, and 140 K exhibits the following time ordered sequence of behavior: an initial blue shift with a loss of the red edge, a broadening of the blue edge, a filling in of the lost red edge, and a continued broadening, which results in the loss of the initial blue shift of the peak wavelength.

The initial blue shift cannot be attributed to tertiary relaxation since the viscosity studies and the Hb* and Mb* spectra at 270 and 260 K all indicate that tertiary relaxation is slowed and indeed stopped at the high viscosity values occurring as the glass transition of glycerol is approached. Instead, KHB is the obvious cause of the blue shift at early times for the same reasons given for the explanation of the temperature-dependent blue shift in the Hb*(10 ns) spectra.

The line broadening that follows KHB is ascribed to thermal fluctuations inducing transitions among energetically similar but spectrally distinct conformational substates. The thermally induced spectral broadening can arise from two similar phenomena. The first is that, at a given temperature, the distribution of initially prepared cs (reflecting the equilibrium distribution of the parent CO bound derivative) can be narrower than the corresponding distribution for the five coordinate species having the same overall tertiary structure. In other words, the effective spring constant for the five and six coordinate species can be different, and hence, the shape of the potential surface can be different. If as Agmon and Sastry (1996) contend that the surface for the five coordinate species is less steep than that of the corresponding six coordinate surface, then initial distribution of cs for the unrelaxed photoproduct can be a nonequilibrium distribution with respect to kT even if the tertiary structures of the five and six coordinate species have the same global minimum. As the thermally accessible but unpopulated cs are accessed through fluctuations, band III will start to adopt the line shape that is commensurate with the shape of the potential surface of the photoproduct. The second but related broadening mechanism is the previously introduced DHF due to thermal fluctuations causing the repopulation of the KHB-induced lost red edge.

Much of the time-dependent line shape changes are interpretable in terms of a combination of the above two effects; however, an additional effect is needed to fully explain the observations. There appears to be a temporal regime during which line broadening is occurring on the blue edge of band III but with no apparent filling in of the red edge "hole". A possible and plausible explanation is that, as the fast rebinding "red edge" cs are being repopulated through thermal fluctuations, they are in effect being rapidly depleted due to fast recombination. The observation that the red edge does eventually recover and broaden beyond the initial width of the 10 ns spectrum suggests that with increasing time there is a slow down of the recombination process for a given cs. A slow down of this kind is hard to understand if the fluctuations are only repopulating the missing red edge cs. The filling in of the red edge must therefore be accompanied by parallel events that result in a progressive slowing down of the rebinding kinetics with respect to the lifetime (interconversion time) of the newly generated fast rebinding cs. The results are clearly not consistent with having the ligand remain positioned near the iron such that at the instant a low barrier cs is regenerated, the ligand rebinds with the same rate that generated the initial KHB.

The observation of dynamic hole filling implies that the fluctuations that regenerate the red edge cs also initiate diffusion away from the iron (i.e., decay of the geminate contact pair). Studies (Carlson et al., 1994, 1996; Gibson et al., 1992; Ikeda-Saito et al., 1993) indicate that the ligand can occupy different thermally accessible sites within the distal pocket subsequent to photodissociation and that the rebinding from these different sites can occur with different rates. It can be reasonably assumed that for a given cs, the fastest rates occur for ligand occupancy of those sites closest to the iron. It follows that a reasonable mechanism for the appearance of DHF is that the same class of fluctuations that help redistribute the cs responsible for KHB also mediate ligand diffusion within the distal hemepocket.

Although the rapid time-dependent decrease in the signal to noise ratio for band III (due to the high geminate yield for COHb) makes quantitative analysis of the line shape difficult, it is still possible to make several conclusions regarding the patterns associated with KHB and DHF. It is clear that KHB persists longer at the lowest temperatures. Furthermore, DHF is clearly occurring at 140 K, which is well below the glass transition. The early KHB studies suggest that DHF is not detectable at temperatures below 100 K.

Potential Surface Collapse and Conformational Diffusion. Agmon, using a temperature-dependent effective potential to analyze the temperature dependence ($\sim$100−300 K) of the geminate rebinding in COMb in 75% glycerol (Agmon & Sastry, 1996) and in a trehalose glass (Sastry & Agmon, 1997), concluded that there are two phenomena that can contribute to the non-Arrhenius inverse temperature effect in which the rebinding kinetics start slowing down with increasing temperature. The first is a relaxation that results in the "collapse" with increasing temperature of the energy difference between the minima of the ligand-bound potential surface and the five coordinate surface. This phenomena occurs at or around the glass transition and is therefore likely to be viscosity dependent. The analysis cannot distinguish whether the six coordinate surface is undergoing a static temperature-dependent shift in energy or whether the surface associated with Mb* is undergoing a rapid relaxation that precedes the onset of rebinding.

The second relaxation is a thermally activated diffusion-like process with little if any dependence on the glass transition. It occurs both in 75% glycerol (Agmon & Sastry, 1996) and trehalose glass (Sastry & Agmon, 1997) over a temperature range extending from ambient to below 140 K but with a different activation energy for the two solvents.

The temperature and viscosity dependence of the band III peak shift for Mb*(10 ns) and of the line broadening bear a resemblance to Agmon's "collapse" and diffusion processes, respectively.

Below ~180 K, Mb*(10 ns) exhibits a red-shifted band III at ~765 nm. Over a relatively narrow temperature regime starting at ~180 K, band III for Mb*(10 ns) in 75% glycerol blue shifts toward the equilibrium deoxy value of ~762 nm. Thus, as the temperature is raised above the glass transition, the Mb*(10 ns) versus deoxy Mb spectral difference is rapidly reduced, following the same overall pattern as Agmon's "collapse" phenomenon. A similar transition is observed with millisecond resolution (Nienhaus et al., 1994), but not surprisingly, the temperature range of the transition is expanded compared to that associated with Mb*(10 ns). In a trehalose glass where there is no collapse (Sastry & Agmon, 1997), the spectral difference between Mb*(10 ns) and deoxy Mb persists even at 300 K (Levin & Friedman, unpublished results).

Since, in the absence of large distal hemepocket alterations (Kiger et al., 1995), the height of the inner kinetic barrier controlling iron−ligand bond formation has been shown through KHB to correlate with the wavelength of band III for a given protein (low barrier-red peak wavelength), it is not surprising that the temperature/viscosity-dependent spectral behavior of Mb*(10 ns) also correlates with the CO rebinding properties in the two solvents. In 75% glycerol, there is the well-established (Austin et al., 1975) inverse temperature effect (slow down in CO rebinding kinetics with increasing temperature) occurring over the same temperature region as the collapse (Agmon & Sastry, 1996). Hagen et al. (1995, 1996) showed that in a trehalose glass there is no discernible inverse temperature effect. It is therefore likely that the collapse is the viscosity-dependent tertiary relaxation of Mb*, responsible for the 765 to 762 nm shift in band III, which precedes the geminate phase at low viscosity but slows to time scales that eventually exceed the onset of geminate rebinding as the viscosity increases. As a consequence, the height of the inner kinetic barrier (or distribution of barriers) is expected to follow the same viscosity dependence as the relaxation dependence of band III.

Hb is expected to show a very different collapse pattern. In contrast to Mb*, where at low viscosity the tertiary relaxation precedes the onset of geminate rebinding, in Hb*, the major segment of relaxation is occurring on the same or slower time scale as the geminate rebinding of CO [see, for example, Scott and Friedman (1984), Sassaroli and Rousseau (1987), and Dunn and Simon (1991)].

The nature of the line-broadening data makes a quantitative analysis difficult at this time. As a consequence, a direct evaluation of the activation energy for the broadening is not feasible and thus a direct comparison of the broadening to Agmon's activated conformational diffusion process is not possible. Nonetheless, the persistence of the line broadening down to comparable temperatures to what is observed by Agmon for the diffusion process makes a case for linking the activated diffusion to the line-broadening phenomena.

Agmon and Sastry (1996) claim that both the collapse and the diffusion process contribute to the inverse temperature effect for geminate rebinding of CO to Mb. As stated above, the slower tertiary relaxation times for Hb* are essentially frozen out at much higher temperatures than in Mb*. As a consequence, the inverse temperature effect for the fast components of GR in Hb* in the region of the glass transition is not due to the slow down of the tertiary relaxation responsible for the shifts in both band III and ν(Fe-His). Instead, it is likely that temperature-dependent changes in the thermal averaging time, which we link to Agmon's diffusional process, is the likely contributor to the inverse temperature effect for the fast geminate phases in Hb*. In the absence of fast averaging there are fast rebinding cs that contribute to the overall rebinding whereas, in the rapid averaging limit, one is left with an average barrier that is clearly higher than those associated with the fast binding populations. The observation of an inverse temperature effect for COHb in a trehalose glass (Gottfried et al., 1996) supports this assessment.

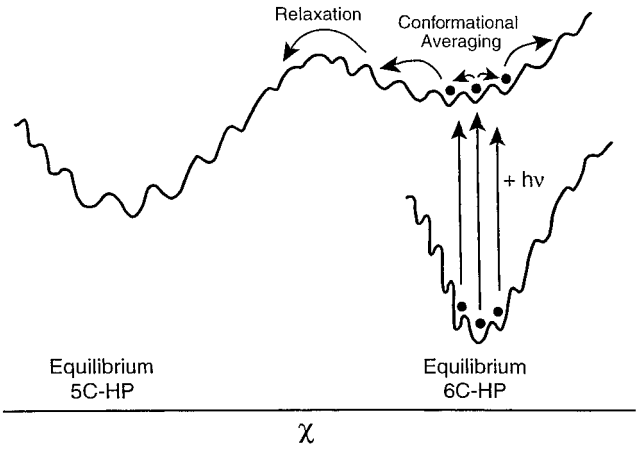

FIGURE 10: A schematic representation of a possible mechanism for time dependent spectral broadening and subsequent relaxation of band III upon photodissociation of a six coordinate heme protein (6C-HP). The local minima on the energy surface correspond to different conformational substates (cs) that have both different band III peak positions and different functional properties. The distribution of cs for the population of 6C-HP at the instant of photodissociation is instantaneously mapped onto the surface of the resulting five coordinate heme protein (5C-HP). The difference in the shape of the two surfaces results in the initial 5C-HP distribution of cs not being a thermalized one and as a consequence it evolves in time.

Evidence for a Hierarchy of Dynamical Processes. Figure 10 depicts the hierarchical picture that is consistent with band III behavior. At the instant of photolysis, the initial distribution of cs is mapped onto the five coordinate surface without any change in the overall protein coordinate, χ. This initial distribution is a nonequilibrium distribution with respect to both χ and the distribution of cs within the local minima associated with the different accessible discrete tertiary states. Frauenfelder has referred to such well-defined discrete cs as taxonomic cs as opposed to the groupings of cs that have a large ill defined membership. Figure 10 shows two minima in the five coordinate surface that can be designated as taxonomic, and each of these has a rough energy landscape that gives rise to a large distribution of the "distributed" or "statistical" cs. The energy barriers separating the taxonomic cs are much larger than those separating the distributed cs, hence the origin of the dynamical hierarchy.

Figure 10 illustrates how KHB, thermal averaging (line broadening), and relaxation (the collapse) are explained within the context of the hierarchy model. The initial distribution is transiently frozen, i.e., inhomogeneous. During this period, KHB is observable if the geminate rebinding occurs during this temporal window. As the initial non-Boltzmann distribution of the distributed (nontaxonomic) cs begins to thermalize, KHB ends and band III broadens. When the temperature is high enough and the viscosity low enough,

the thermalized distribution of cs can relax toward the equilibrium taxonomic state. As the taxonomic cs relaxation proceeds, the distribution of distributed cs adiabatically adjusts to the new globin-induced constraints. Each taxonomic cs has its own energy landscape that dictates the energies and hence the distribution of the lower tier distributed cs.

Origin of Stretched Exponential Relaxation Kinetics. Anfinrud and co-workers (Lim et al., 1993) have shown that the relaxation of Mb* at 300 K follows stretched exponential kinetics. Even though the largest shifts in band III are over within less than a nanosecond, relaxation continues out to hundreds of nanoseconds or longer. This observation suggests either of two models for relaxation. One model follows from surfaces of the kind seen in Figure 10 in that the activation energy for relaxation for each cs in the unrelaxed well is different based on the transition state energy being approximately the same but the well depth for each cs being different. Such a model has been proposed by Hagen and Eaton (1996). The problem with this model as it applies to high-temperature behavior is that thermal averaging of the distributed cs occurs much faster than the overall tertiary relaxation time as determined both from DHF and double pulse studies (Tian et al., 1992, 1996). As a consequence, there should only be an average barrier for relaxation. Alternative models that account for the stretched exponential kinetics at higher temperatures include (1) there being a series of wells (due to multiple taxonomic cs for a given protein coordinate) separated by barriers that get larger as the relaxation progresses towards equilibrium; (2) there being a slowly interconverting distribution of solvated protein molecules with each distinct solvated member of the distribution having a different double-welled potential surface (based on the solvent shell) that has a different rate of relaxation; and (3) there being several independent structural degrees of freedom that contribute to the peak shifts in the absorption bands and these different degrees of freedom have different relaxation time constants. Given the substantial viscosity dependence of the taxonomic relaxation, the second possibility, which has the hydration sphere influencing dynamics, is likely to contribute to the stretched exponential time dependence.

ACKNOWLEDGMENT

J.M.F. wishes to thank M. Pereira for the use of his femtosecond apparatus for the picosecond geminate rebinding measurements and N. Agmon, H. Frauenfelder, and U. Nienhaus for helpful comments.

REFERENCES

Abadan, Y., Chien, E. Y. T., Chu, K., Eng, C. D., Nienhaus, G. U., & Sligar, S. G. (1995) *Biophys. J. 68*, 2497−2504.

Agmon, N. (1988) *Biochemistry 27*, 3507−3511.

Agmon, N. (1990) in *Dynamical Processes in Condensed Molecular Systems. Proceedings of the Emil Warburg Symposium* (Blumen, A., Klafter, J., & Haarer, D., Eds.) pp 333−347, World Scientific, Singapore.

Agmon, N., & Hopfield, J. J. (1983) *J. Chem. Phys. 79*, 2042−2053.

Agmon, N., & Sastry, M. (1996) *Chem. Phys. 212*, 207−219.

Ahmed, A. M., Campbell, B. F., Caruso, D., Chance, M. R., Chavez, M. D., Courtney, S.H., Friedman, J. M., Iben I. E. T., Ondrias, M. R., & Yang M. (1991) *Chem. Phys. 158*, 329−351.

Alpert, B., El Mohsni, Lindqvist, J., & Tfibel, F. (1979) *Chem Phys. Lett. 64*, 11−16.

Ansari, A., Berendzen, J., Bowne, S. F., Frauenfelder, I. E. T., Iben, Sauke, T. B., Shysamunder, E., & Young, R. D. (1985) *Proc. Natl. Acad. Sci. U.S.A. 85*, 5000−5004.

Ansari, A., Berendzen, J., Braunstein, D., Cowen, B. J., Frauenfelder, H., Hong, M. K., Iben, I. E. T., Johnson, B. J., Ormos, P., Sauke, T. B., Scholl, R., Schulte, A., Steinbach, P. J., Vittitow, J., & Young, R. D. (1987) *Biophys. Chem. 26*, 337−355.

Ansari, A., Jones, C. M., Henry, E. R., Hofrichter, J., & Eaton, Wm. A. (1992) *Science 256*, 1796−1798.

Ansari, A., Jones, C. M., Henry, E. R., Hofrichter, J., & Eaton, W. A. (1994) *Biochemistry 33*, 5128−5145.

Austin, R. H., Beeson, K. W., Einstein, L., Frauenfelder, H., & Gunsalus, I. C. (1975) *Biochemistry 14*, 5355−5373.

Campbell, B. F., Chance, M. R., & Friedman, J. M. (1987) *Science 238*, 373−376.

Carlson, M. L, Regan, R., Elber, R., Li, H., Phillips, G. N., Jr, Olson, J. S., & Gibson, Q. H. (1994) *Biochemistry 33*, 10597−10606.

Carlson, M. L., Regan, R. M., & Gibson, Q. H. (1996) *Biochemistry 35*, 1125−1136.

Chavez, M. D., Courtney, S. H., Chance, M. R., Kiula, D., Nocek, J., Hoffman, B. M., Friedman, J. M., & Ondrias, M. R. (1990) *Biochemistry 429*, 4844−4852.

Cordone, L., Cupane, A., Leone, M., & Vitrano, E. (1986) *Biophys. Chem. 24*, 259−275.

Cupane, A., Leone, M., Vitrano, E., & Cordone, L. (1988) *Biopolymers 27*, 1977−1985.

Duddell, D. A., Morris, R. J., & Richards, J. T. (1979) *J. Chem. Soc., Chem. Commun.* 75−76.

Dunn, R. C., & Simon, J. D. (1991) *Biophys. J. 60*, 884−889.

Eaton, W. A., Hanson, L. K., Stephens, P. J., Sutherland, J. C., & Dunn, J. B. R. (1978) *J. Am. Chem. Soc. 100*, 4991−5003.

Findsen, E. W., Friedman, J. M., & Ondrias, M. R. (1988) *Biochemistry 27*, 8719−8724.

Franzen, S., & Boxer, S. G. (1997) *J. Biol. Chem. 272*, 9655−9660.

Frauenfelder, H. (1995) *Nat. Struct. Biol. 2*, 821−823.

Frauenfelder, H., & Wolynes, P. G. (1985) *Science 229*, 337−345.

Frauenfelder, H., Parak, F., & Young, R. D. (1988) *Annu. Rev. Biophys. Biochem. 17*, 451−479.

Frauenfelder, H., Sligar, S. G., & Wolynes, P. G. (1991) *Science 254*, 1598−1603.

Friedman, J. M. (1985) *Science 228*, 1273−1280.

Friedman, J. M. (1994) *Methods Enzymol. 232*, 205−231.

Friedman, J. M., & Lyons, K. B. (1980) *Nature 284*, 570−572.

Friedman, J. M., Scott, T. W., Fisanick, G. J., Simon, S. R., Findsen, E. W., Ondrias, M. R., & MacDonald, V. W. (1985) *Science 229*, 187−190.

Gibson, Q. H., Regan, R., Elber, R., Olson, J. S., & Carver, T. E. (1992) *J. Biol. Chem. 267*, 22022−22034.

Gilch, H., Schweitzer-Stenner, R., Dreybrodt, Leone, M., Cupane, A., & Cordone, L. (1996) *Int. J. Quant. Chem. 59*, 301−313.

Gottfried, D. S., Peterson, E. S., Sheikh, A. G., Wang, J., Yang, M., & Friedman, J. M. (1996) *J. Phys. Chem. 100*, 12034−12042.

Greene, B., Hochstrasser, R. M., Weisman, R. B., & Eaton, W. A. (1978) *Proc. Natl. Acad. Sci. U.S.A. 75*, 5255−5259.

Hagen, S. J., & Eaton, W. A. (1996) *J. Chem. Phys. 104*, 3395.

Hagen, S. J., Hofrichter, J., & Eaton, W. A. (1995) *Science 269*, 959−962.

Hagen, S. J., Hofrichter, J., & Eaton, W. A. (1996) *J. Phys. Chem. 100*, 12008−12021.

Henry, E. R., Sommer, J. H., Hofrichter, J., & Eaton, W. A. (1983) *J. Mol. Biol. 166*, 443−451.

Hofrichter, J., Sommer, J. H., Henry, E. R., & Eaton, W. A. (1983) *Proc. Natl. Acad. Sci. U.S.A. 80*, 2235−2239.

Huang , J., Leone, M., Boffi, A., Friedman, J. M., & Chianconi, E. (1996) *Biophys. J. 70*, 2924−2929.

Iben, I. E. T., Braunstein, D., Doster, W., Frauenfelder, H., Hong, H., Johnson, J., Luck, S., Ormos, P., Schulte, A., Steinbach, P., Xie, A., & Young, R. D. (1989) *Phys. Rev. Lett. 62*, 1916−1919.

Ikeda-Saito, M., Dou, Y., Yonetani, T., Olson, J. S., Li, T., Regan, R., & Gibson, Q. H. (1993) *J. Biol. Chem. 268*, 6855−6857.

Izuka, T., Yamamoto, H., Kotani, M., & Yonetani, T. (1974) *Biochem. Biophys. Acta. 371*, 126−139.
Jackson, T. A., Lim, M., & Anfinrud, P. A. (1993) *Chem. Phys. 180*, 131−140.
Jayaraman, V., Rodgers, K. R., Mukerji, I., & Spiro, T. G. (1995) *Science 269*, 1843.
Jongeward, K. A., Magde, D., Taube, D. J., Marsters, J. C., Traylor, T. G., & Sharma, V. S. (1988) *J. Am. Chem. Soc. 110*, 380−387.
Kiger, L., Stetzkowsi-Marden, F., Poyart, C., & Marden, M. J. (1995) *Eur. J. Biochem. 228*, 665−668.
Leeson, D. T., & Wiersma, D. A. (1995) *Nat. Struct. Biol. 2*, 848−851.
Lim, M., Jackson, T. A., & Anfinrud, P. A. (1993) *Proc. Natl. Acad. Sci. U.S.A. 90*, 5801−5804.
Martin, J. L., Migus, A., Poyart, C., Lecarpentier, Y., Astier, R., & Antonetti, A. (1983) *Proc. Natl. Acad. Sci. U.S.A. 80*, 173−177.
Murray, L. P., Hofrichter, J., Henry, E. R., & Eaton, W. A. (1988) *Biophys. Chem. 29*, 63−76.
Nienhaus, G. U., Morant, J. R., & Frauenfelder, H. (1992) *Proc. Natl. Acad. Sci. U.S.A. 89*, 2902−2906.
Nienhaus, G. U., Mourant, J. R., Chu, K., & Frauenfelder, H. (1994) *Biochemistry 33*, 13413−13430.
Olson, J. S., & Phillips, G. N., Jr. (1996) *J. Biol. Chem. 271*, 17593−17596.
Rohlfs, R. J., Olson, J. S., & Gibson, Q. H. (1988) *J. Biol. Chem. 263*, 1803−1813.
Sage, J. T., Schomacker, K. T., & Champion, P. M. (1995) *J. Phys. Chem. 99*, 3394−3405.
Sassaroli, M., & Rousseau, D. L. (1987) *Biochemistry 26*, 3092−3098.
Sastry, M., & Agmon, N. (1997) *Biochemistry* (in press).
Scott, T. W., & Friedman, J. M. (1984) *J. Am. Chem. Soc. 106*, 5677−5687.
Scott, T. W., Friedman, J. M., & Macdonald, V. W. (1985) *J. Am. Chem. Soc. 107*, 3702−3705.
Srajer, V., & Champion, P. M. (1991) *Biochemistry 30*, 7390−7402.
Steinbach, P. J., Ansari, A., Berendzen, J., Braunstein, D., Chu, K., Cowen, B. R., Ehrenstein, D., Frauenfelder, H., Johnson, B., Lamb, D. C., Luck, S., Mourant, J. R., Nienhaus, G. U., Ormos, P., Philipp, R., Xie, A., & Young, R. D. (1991) *Biochemistry 30*, 3988−4001.
Tian, W. D., Sage, J. T., Srajer, V., & Champion, P. M. (1992) *Phys. Rev. Lett. 68*, 3408−411.
Tian, W. D., Sage, J. T., Champion, P. M, Chien, E., & Sligar, S. G. (1996) *Biochemistry 35*, 3487−3502.

BI9700274